Journal of Materials Chemistry A

COMMUNICATION

View Article Online
View Journal | View Issue

Cite this: J. Mater. Chem. A, 2017, 5, 16590

Received 9th June 2017
Accepted 18th July 2017

DOI: 10.1039/c7ta05007k

rsc.li/materials-a

Superior sodium storage performance of additive-free V_2O_5 thin film electrodes†

Yanwei Li,[a] Canzheng Liu,[a] Zhiping Xie,[a] Jinhuan Yao*[a] and Guozhong Cao*[b]

A binder- and conductive-agent-free V_2O_5 thin film electrode was fabricated by a facile and cost-efficient cathodic deposition method directly on stainless steel substrates followed by annealing at 300 °C in air for 1 h. The V_2O_5 film is approximately 1 μm in thickness and consists of layer-by-layer stacked nanosheets. When used as a cathode for sodium ion batteries, the V_2O_5 thin film electrode exhibits a high reversible discharge capacity (174 mA h g^{-1} at 200 mA g^{-1}), excellent cycling stability (almost 100% capacity retention over 200 cycles at 1 A g^{-1}), and outstanding rate capability (retaining a capacity of 124 mA h g^{-1} at 5 A g^{-1}). Cyclic voltammetric analyses reveal that pseudocapacity-dominated charge storage of sodium ions accounts for the superior performance.

Introduction

Sodium ion batteries (SIBs) have been considered as promising next-generation alternatives to lithium-ion batteries (LIBs), because sodium is widely available, low cost, and environmentally friendly, and exhibits similar chemistry to lithium.[1] However, compared to LIBs, the larger radius (0.98 Å) of Na^+ leads to sluggish electrochemical reaction kinetics and unsatisfactory cycling stability of the electrode.[2] Therefore, the development and optimization of electrode materials that can effectively and reversibly accommodate Na^+ is desperately needed. Currently, many efforts have been devoted to developing new cathode materials for SIBs, such as transition-metal oxides, polyanionic compounds, metal hexacyanometalates, and organic compounds.[3] Among the potential cathode materials for SIBs, layer structured vanadium pentoxide (V_2O_5) has attracted increasing attention due to its simple structure, abundance in nature, ease of synthesis, and high theoretical capacity (236 mA h g^{-1}).[4–12] Unfortunately, structural deterioration (the collapse of the layered structure during repeated Na^+ insertion/extraction between the layers) and slow electrochemical kinetics are still major challenges for the practical application of V_2O_5 in SIBs.[6] Engineering materials at the nanoscale offers unique electrode properties, such as an increased contact area between the electrolyte and electrode, short ion transport pathways, and better accommodation of strains, leading to enhanced electrochemical energy storage properties of batteries.[3,13–15] Several different types of V_2O_5 nanostructures, such as hierarchical hollow nanospheres,[10] nanobelts,[11] and nanosheets[5] have been synthesized and they exhibited enhanced sodium storage performance. However, most of the previously reported nanostructured V_2O_5 is in powder form and needs to be mixed with a polymer binder and carbon black, and finally pasted onto a current collector, which inevitably sacrifices the energy density of the whole electrodes. Moreover, the binder involved will greatly decrease the electronic conductivity of the electrode materials, hindering the fast electron transport required for excellent cycling ability and rate capability. Recently, a new strategy to construct additive-free electrodes with satisfactory electric conductivity and self-integrity has been exploited for boosting the storage performance of electrode materials.[16–18]

Herein, we demonstrate a facile approach to fabricate an additive-free V_2O_5 thin film electrode through a simple cathodic deposition method and subsequent annealing in air. The film is composed of stacked ultra-thin nanosheets (~10 nm) parallel to the substrate. When applied as an electrode for SIBs, this additive-free V_2O_5 electrode exhibited high sodium storage activity, excellent cycling stability, and impressive rate capability due to its unique stacked layer nanostructure and pseudocapacity dominated charge storage of sodium ions.

[a]Guangxi Key Laboratory of Electrochemical and Magneto-Chemical Function Materials, College of Chemistry and Bioengineering, Guilin University of Technology, Guilin 541004, China. E-mail: yaojinhuan@126.com

[b]Department of Materials Science and Engineering, University of Washington, Seattle, Washington 98195, USA. E-mail: gzcao@uw.edu

† Electronic supplementary information (ESI) available. See DOI: 10.1039/c7ta05007k

Experimental

Preparation of V_2O_5 thin film electrodes

The V_2O_5 thin film electrodes were prepared by a cost-effective cathodic deposition method from diluted V_2O_5 solutions, which were made according to the procedure reported by Fontenot *et al.*[19] In brief, V_2O_5 powders (AR, Shantou Xilong Chemical Factory, China) were added into deionized water and H_2O_2 (30 wt% in H_2O, Shantou Xilong Chemical Factory, China) to obtain a solution with a V_2O_5 concentration (C_V) of 0.3 M and $n(H_2O_2) : n(V)$ of 8 : 1. The resulting solution was stirred and sonicated for 15 min successively, followed by dilution to C_V = 0.056 M and then sonication for 90 min until the solution turned into brownish red V_2O_5 gel. This gel was further dispersed and diluted by deionized water to form a brick-red colored, transparent solution with a C_V of 0.008 M and used as the deposition precursor. For the preparation of V_2O_5 thin films, a stainless steel sheet (sus.304) was used as the deposition substrate on the negative side, and a Pt plate was used as a counter electrode on the positive side. The deposition voltage was −2.5 V. The as-deposited thin film electrodes were ambient dried and then annealed at 300 °C for 1 h in air.

Materials characterization

The microstructures of the V_2O_5 thin films were characterized by X-ray diffraction (XRD, PANalytical, X'Pert^3 powder), field emission scanning electron microscopy (SEM, HITACHI, SU5000), and transmission electron microscopy (TEM, JEOL, JEM-2100F). The oxidation state of V in the V_2O_5 thin film was determined with an X-ray photoelectron spectrometer (XPS, Thermo Electron Corp, ESCALAB 250Xi). Thermogravimetric analysis (TGA) measurement was carried out using a thermogravimetric analyzer (TA instruments, SDT Q600) at a ramp rate of 10 °C min^{-1} in air from ~25 to 600 °C.

Electrochemical measurement

The sodium storage performance of the V_2O_5 thin film electrode (the mass loading was ~0.5 mg cm^{-2}) was tested using a sealed standard three-electrode setup with a Pt plate as the counter electrode, Ag/Ag^+ as the reference electrode, and 1 M $NaClO_4$ in propylene carbonate (PC) as the electrolyte. The rate capability and cycling performance were investigated by a chronopotentiometry (CP) method. The cyclic voltammetry (CV) curves were measured with a scan rate ranging from 5 to 25 mV s^{-1}. Both CV and CP tests were performed using an electrochemical analyzer (CH Instruments, Model 760E) in the voltage range between −1.50 and 0.50 V (*vs.* Ag/Ag^+).

Results and discussion

Fig. 1a presents the XRD patterns of the V_2O_5 film electrode before cycling and after 200 discharge/charge cycles at a current density of 1.0 A g^{-1}. Before cycling, the film electrode shows typical (001) reflection peaks, which agree well with the layered $V_2O_5 \cdot nH_2O$ (JCPDS no. 40-1296).[5] The interlayer distance is estimated to be 11.2 Å by Bragg's law from the (001) peak position. This huge distance is beneficial for Na^+ insertion/extraction.[11] After 200 cycles, the peak shape and relative intensity are almost the same as those before cycling, which means that the layered structure was well retained after repeated Na^+ insertion/extraction cycles. However, the position of the (001) peaks moved to a higher angle. The calculated interlayer distance decreased to 10.8 Å. This contraction of the interlayer distance can be due to the inserted Na^+ which exerts electrostatic attraction with the vanadium oxygen pyramids. In the initial several discharge/charge cycles, quite some Na^+ did not come out from the V_2O_5 film electrode as reflected by the coulombic efficiency shown in Fig. 2d. The XPS result (Fig. S3a†) of the V_2O_5 film in the fully charged state also confirms that quite some Na^+ was trapped in the V_2O_5 film after discharge/charge cycles. The size of the crystalline domains along the (001) facet is calculated to be ~10 nm by Scherrer's formula; this value is equal to the average thickness of the nanosheets as shown in Fig. 1f. To identify the oxidation state of vanadium in the as-prepared V_2O_5 film, XPS was carried out and the result is shown in Fig. 1b. The V $2p_{3/2}$ state has a broad peak and can be deconvoluted into two binding energies: 517.43 and 516.05 eV, corresponding to V^{5+} and V^{4+}, respectively.[16] The V^{4+}/V^{5+} ratio is 16.33%, indicating the presence of oxygen vacancies in the V_2O_5 lattice. Previous studies on V_2O_5 for LIBs demonstrated that such vacancies may enhance the electrochemical performance.[20,21] From the TGA plot (Fig. 1c) of the V_2O_5 film, the composition of the film is estimated to be $V_2O_5 \cdot 0.58H_2O$. Fig. 1d–h show the SEM images of the V_2O_5 film before cycling and after 200 discharge/charge cycles at a current density of 1.0 A g^{-1}. Before cycling, the V_2O_5 film exhibits a smooth surface morphology, which is composed of fiber-like nanostructures with a width narrower than 100 nm. This fiber-like surface morphology could be related to the formation of hydrous V_2O_5 as reported in the previous literature.[16,22] The inset of Fig. 1d shows that the electrode is highly flexible. After 200 cycles, the surface of the V_2O_5 film gets rough and the fiber-like nanostructures become more obvious. Nanopores between the densely packed nanofibers can be clearly observed on the surface of the film (Fig. 1g), which will facilitate the penetration of electrolyte. The cross sectional view of the V_2O_5 films shows a very thin layer-by-layer stacked nanostructure (Fig. 1e and f). The thickness of stacked nanosheets in the V_2O_5 film is ~10 nm, which is in good agreement with the value calculated from XRD results (Fig. 1a). After 200 cycles, the layer-by-layer stacked nanosheet morphology is well retained (Fig. 1h). These very thin nanosheets and the layer-by-layer stacked structures are expected to be advantageous for obtaining good electrochemical performance for SIBs. The TEM images further confirms the nanosheet morphology (Fig. 1i) and the lattice fringe of ~11.2 Å can be assigned to the (001) plane (inset of Fig. 1i), consistent with the XRD pattern (Fig. 1a). The curling up at the edges of the nanosheets suggests their ultrathin feature and good flexibility.

Fig. 2a and b show the rate performance of the V_2O_5 electrode. Even at a very high current density of 5.0 A g^{-1}, the V_2O_5 can still deliver a high discharge capacity of 124 mA h g^{-1}, suggesting its outstanding rate capability. This rate performance is better than those of nanostructured V_2O_5 electrode

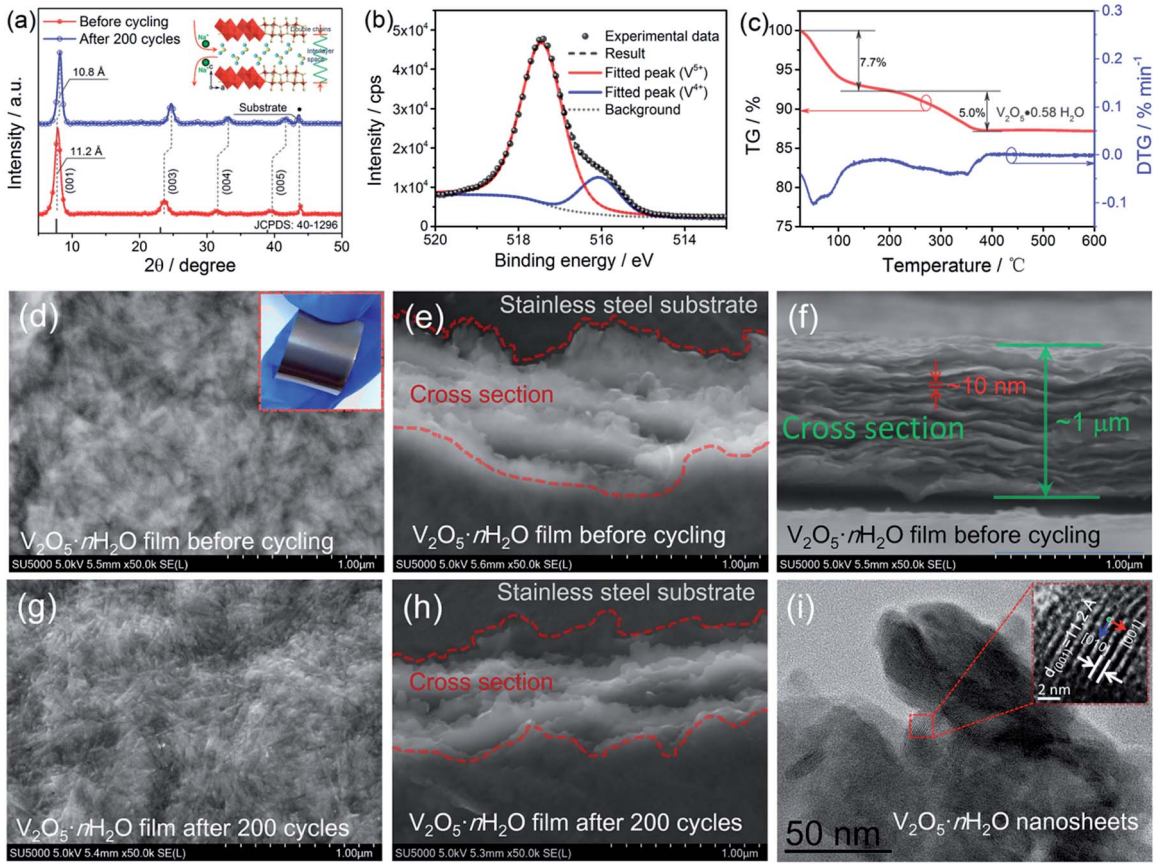

Fig. 1 (a) XRD patterns of the V_2O_5 film before cycling and after 200 cycles. (b) XPS V $2p_{3/2}$ spectrum and (c) TG/DTG plots of the as-prepared V_2O_5 thin film electrode. (d)–(h) SEM images of the V_2O_5 thin film electrode before cycling and after 200 discharge/charge cycles. (i) TEM images of the V_2O_5 nanosheets peeled from the V_2O_5 film.

materials reported in the literature (Fig. 2c).[5–7,9–11,23] Fig. 2d shows the cycling performance of the V_2O_5 electrodes at a current of density of 1.0 A g^{-1}. The discharge capacities increased progressively from 125 to 157 mA h g^{-1} in the initial 30 cycles. This continuous capacity increase during the initial 30 cycles is attributable to the gradual electrochemical activation of the electrode.[16,24] After the 30th cycle, the discharge capacities become stable and there is no capacity decay from the 30th cycle to the 200th cycle. The structural changes of the V_2O_5 film at various depths of discharge (DOD) were monitored by *ex situ* XRD measurement and the results are shown in Fig. 2f and g. With DOD increasing from 0% to 100%, the main (001) diffraction peak shifted toward higher angles along with the decrease in crystallinity (Fig. 2f). The shifting to higher angles reflects the decrease of the interlayer distance (Fig. 2g), which is caused by the coordination reaction of inserted Na^+ with the V_2O_5 skeleton.[6,12] In the charge process, with the depths of charge (DOC) increasing from 0% to 100%, the main (001) diffraction peak shifted toward lower angles along with the increase in crystallinity (Fig. S1†). As shown in Fig. S2,† the changes of the interlayer distance between the discharge (insertion) and the charge (extraction) process show a mirror image. After 200 discharge/charge cycles, the interlayer distance can still recover the value as that in the 10th cycle (Fig. 2g), implying the excellent structural reversibility of the V_2O_5 film during long-term cycling.

Due to the layer-by-layer stacked nanosheet morphology, we expect that the V_2O_5 film electrode may exhibit significant pseudocapacitance.[25–27] According to the sweep voltammetry method proposed by Dunn's group,[28] one can use the scan-rate-dependent CV curves (Fig. 3a) to quantify the contributions from the capacitive effect (k_1v) and diffusion-controlled ($k_2v^{1/2}$) process to the current response using the following equation: $i(V) = k_1v + k_2v^{1/2}$. By determining k_1 and k_2, the capacitive charge storage at a certain voltage can be estimated (Fig. 3b–d). As shown in Fig. 3e, the Na^+ storage in the V_2O_5 film is a capacitive-dominated process, particularly at high scan rates. At 5 mV s^{-1}, the capacitive process accounts for ~57% of the total charge storage, estimated by the enclosed area, while at 25 mV s^{-1}, this value increases to ~75%. To further distinguish pseudocapacitive behavior from the double layer capacitance, we performed CV measurement in an electrolyte with very large ions (1.0 M tetrabutylammonium perchlorate ($TBAClO_4$) in PC) that cannot be inserted into V_2O_5. The obtained capacitance in $TBAClO_4$/PC electrolyte is only 5.2% of the total charge storage, indicating that the majority of the capacitive charge storage is due to the pseudocapacitance (Fig. 3f). Such a high fraction of pseudocapacity can be due to the stacked ultrathin nanosheet

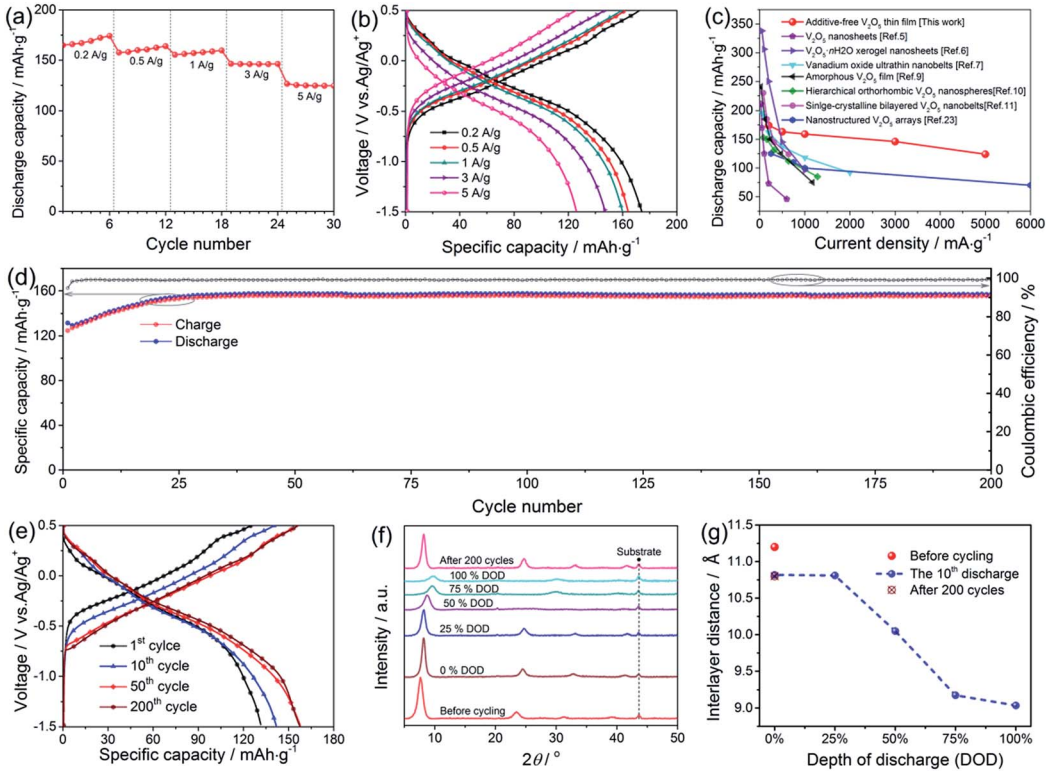

Fig. 2 (a) Rate performance and (b) selected discharge/charge profiles of the V_2O_5 film electrode under various current densities. (c) Comparison of the rate capabilities of the V_2O_5 reported in this work and those in previous literature. (d) Cycling performance and (e) selected discharge/charge profiles of the V_2O_5 film electrode at a current of density of 1.0 A g^{-1}. (f) *Ex situ* XRD patterns and (g) the calculated interlayer distances of the V_2O_5 film at various depths of discharge (DOD).

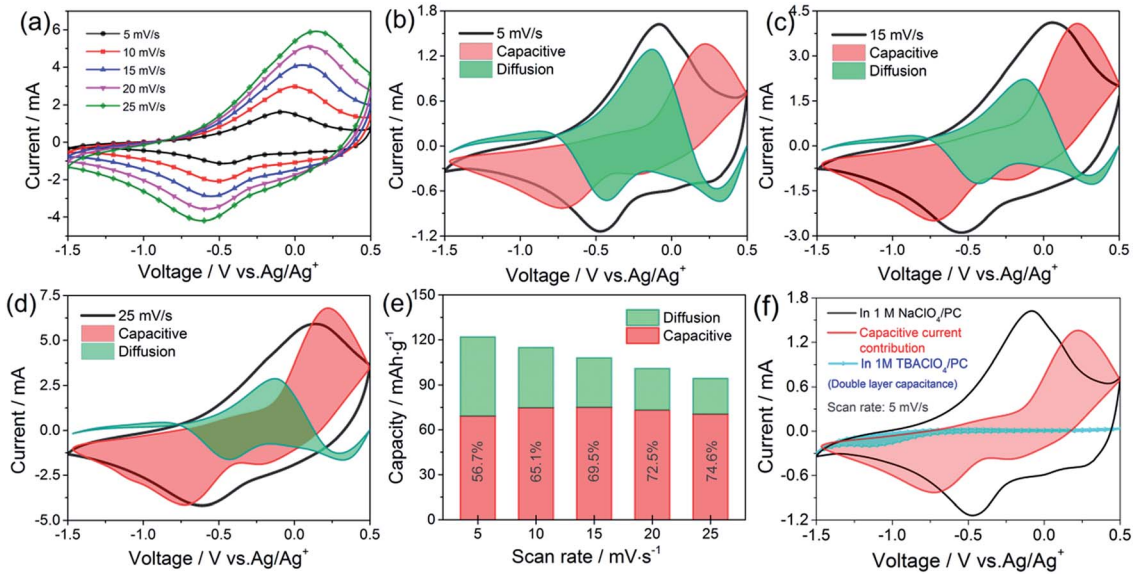

Fig. 3 (a) CV curves of the V_2O_5 film electrode at various scan rates. (b)–(d) Capacitive and diffusion contributions to the total stored charge at different sweep rates. (e) Separation of contributions from capacitive and diffusion-controlled capacities at different sweep rates. (f) CV curves of the V_2O_5 film electrode measured in different electrolytes.

morphology and the presence of oxygen vacancies, which can simultaneously promote Na^+ and electron accessibility to the surface/subsurface. A key feature of pseudocapacitance is that the electrode materials do not undergo phase transitions in association with charge storage,[29] which facilitates fast kinetics and long cycle lifetimes.[27,30–32]

Conclusions

An additive-free V_2O_5 film electrode was fabricated by a very facile and cost-efficient cathodic deposition method. The prepared V_2O_5 film electrode exhibits a high reversible discharge capacity, excellent cycling stability, and outstanding rate capability for Na^+ intercalation/deintercalation. The excellent Na^+ storage performance could be attributed to its unique stacked nanosheet morphology and huge interlayer distance, which could benefit the penetration of the electrolyte, greatly shorten the diffusion path for both Na^+ and electrons, enhance the diffusivity of Na^+ in the electrode, and effectively accommodate the severe volume variation of the electrode material upon cycling. More importantly, kinetic analysis reveals that the Na^+ storage in the V_2O_5 film is a pseudocapacitive-dominated process, which ensures the fast insertion and extraction of Na^+ at a high rate.

Acknowledgements

This work was supported by the National Natural Science Foundation of China (51664012 and 51464009) and Guangxi Natural Science Foundation of China (2015GXNSFGA139006).

Notes and references

1 N. Yabuuchi, K. Kubota, M. Dahbi and S. Komaba, *Chem. Rev.*, 2014, **114**, 11636–11682.
2 R. C. Massé, E. Uchaker and G. Cao, *Sci. China Mater.*, 2015, **58**, 715–766.
3 X. Xiang, K. Zhang and J. Chen, *Adv. Mater.*, 2015, **27**, 5343–5364.
4 G. Ali, J. H. Lee, S. H. Oh, B. W. Cho, K. W. Nam and K. Y. Chung, *ACS Appl. Mater. Interfaces*, 2016, **8**, 6032–6039.
5 K. Zhu, C. Zhang, S. Guo, H. Yu, K. Liao, G. Chen, Y. Wei and H. Zhou, *ChemElectroChem*, 2015, **2**, 1660–1664.
6 Q. Wei, J. Liu, W. Feng, J. Sheng, X. Tian, L. He, Q. An and L. Mai, *J. Mater. Chem. A*, 2015, **3**, 8070–8075.
7 Q. Wei, Z. Jiang, S. Tan, Q. Li, L. Huang, M. Yan, L. Zhou, Q. An and L. Mai, *ACS Appl. Mater. Interfaces*, 2015, **7**, 18211–18217.
8 D. Su, S. Dou and G. Wang, *ChemSusChem*, 2015, **8**, 2877–2882.
9 E. Uchaker, Y. Z. Zheng, S. Li, S. L. Candelaria, S. Hu and G. Z. Cao, *J. Mater. Chem. A*, 2014, **2**, 18208–18214.
10 D. Su, S. Dou and G. Wang, *J. Mater. Chem. A*, 2014, **2**, 11185.
11 D. Su and G. Wang, *ACS Nano*, 2013, **7**, 11218–11226.
12 S. Tepavcevic, H. Xiong, V. R. Stamenkovic, X. Zuo, M. Balasubramanian, V. B. Prakapenka, C. S. Johnson and T. Rajh, *ACS Nano*, 2012, **6**, 530–538.
13 Q. Zhang, E. Uchaker, S. L. Candelaria and G. Cao, *Chem. Soc. Rev.*, 2013, **42**, 3127–3171.
14 A. S. Aricò, P. Bruce, B. Scrosati, J.-M. Tarascon and W. V. Schalkwijk, *Nat. Mater.*, 2005, **4**, 366–377.
15 F. Wang, X. Wu, C. Li, Y. Zhu, L. Fu, Y. Wu and X. Liu, *Energy Environ. Sci.*, 2016, **9**, 3570–3611.
16 Y. Li, J. Yao, E. Uchaker, M. Zhang, J. Tian, X. Liu and G. Cao, *J. Phys. Chem. C*, 2013, **117**, 23507–23514.
17 A. K. Haridas, B. Gangaja, P. Srikrishnarka, G. E. Unni, A. S. Nair, S. V. Nair and D. Santhanagopalan, *J. Power Sources*, 2017, **345**, 50–58.
18 W. Luo, A. Calas, C. Tang, F. Li, L. Zhou and L. Mai, *ACS Appl. Mater. Interfaces*, 2016, **8**, 35219–35226.
19 C. J. Fontenot, J. W. Wiench, M. Pruski and G. L. Schrader, *J. Phys. Chem. B*, 2000, **104**, 11622–11631.
20 D. Liu, Y. Liu, A. Pan, K. P. Nagle, G. T. Seidler, Y.-H. Jeong and G. Cao, *J. Phys. Chem. C*, 2011, **115**, 4959–4965.
21 X. Peng, X. Zhang, L. Wang, L. Hu, S. H.-S. Cheng, C. Huang, B. Gao, F. Ma, K. Huo and P. K. Chu, *Adv. Funct. Mater.*, 2016, **26**, 784–791.
22 V. Petkov, P. N. Trikalitis, E. S. Bozin, S. J. L. Billinge, T. Vogt and M. G. Kanatzidis, *J. Am. Chem. Soc.*, 2002, **124**, 10157–10162.
23 H. Wang, X. Gao, J. Feng and S. Xiong, *Electrochim. Acta*, 2015, **182**, 769–774.
24 C. Peng, B. Chen, Y. Qin, S. Yang, C. Li, Y. Zuo, S. Liu and J. Yang, *ACS Nano*, 2012, **6**, 1074–1081.
25 V. Raju, J. Rains, C. Gates, W. Luo, X. Wang, W. F. Stickle, G. D. Stucky and X. Ji, *Nano Lett.*, 2014, **14**, 4119–4124.
26 M. Sathiya, A. S. Prakash, K. Ramesha, J. M. Tarascon and A. K. Shukla, *J. Am. Chem. Soc.*, 2011, **133**, 16291–16299.
27 W. Dong, D. R. Rolison and B. Dunn, *Electrochem. Solid-State Lett.*, 2000, **3**, 457–459.
28 J. Wang, J. Polleux, J. Lim and B. Dunn, *J. Phys. Chem. C*, 2007, **111**, 14925–14931.
29 H. S. Kim, J. B. Cook, S. H. Tolbert and B. Dunn, *J. Electrochem. Soc.*, 2015, **162**, A5083–A5090.
30 V. Augustyn, J. Come, M. A. Lowe, J. W. Kim, P. L. Taberna, S. H. Tolbert, H. D. Abruna, P. Simon and B. Dunn, *Nat. Mater.*, 2013, **12**, 518–522.
31 Z. Chen, V. Augustyn, J. Wen, Y. Zhang, M. Shen, B. Dunn and Y. Lu, *Adv. Mater.*, 2011, **23**, 791–795.
32 J. B. Cook, H.-S. Kim, Y. Yan, J. S. Ko, S. Robbennolt, B. Dunn and S. H. Tolbert, *Adv. Energy Mater.*, 2016, **6**, 1501937.

